Journal of Microscopy

Journal of Microscopy, Vol. 245, Pt 3 2012, pp. 245–251
Received 11 July 2011; accepted 9 October 2011

doi: 10.1111/j.1365-2818.2011.03566.x

Transmission EBSD from 10 nm domains in a scanning electron microscope

R.R. KELLER & R.H. GEISS
Materials Reliability Division, National Institute of Standards and Technology, Boulder, CO 80305, U.S.A.

Key words. Crystallography, EBSD, nanoparticle analysis, SEM, transmission EBSD, ultrathin film analysis.

Summary

The spatial resolution of electron diffraction within the scanning electron microscope (SEM) has progressed from channelling methods capable of measuring crystallographic characteristics from 10 μm regions to electron backscatter diffraction (EBSD) methods capable of measuring 120 nm particles. Here, we report a new form of low-energy transmission Kikuchi diffraction, performed in the SEM. Transmission-EBSD (t-EBSD) makes use of an EBSD detector and software to capture and analyse the angular intensity variation in large-angle forward scattering of electrons in transmission, without postspecimen coils. We collected t-EBSD patterns from Fe–Co nanoparticles of diameter 10 nm and from 40 nm-thick Ni films with in-plane grain size 15 nm. The patterns exhibited contrast similar to that seen in EBSD, but are formed in transmission. Monte Carlo scattering simulations showed that in addition to the order of magnitude improvement in spatial resolution from isolated particles, the energy width of the scattered electrons in t-EBSD is nearly two orders of magnitude narrower than that of conventional EBSD. This new low-energy transmission diffraction approach builds upon recent progress in achieving unprecedented levels of imaging resolution for materials characterization in the SEM by adding high-spatial-resolution analytical capabilities.

Introduction

The measurement of characteristics such as crystal structure, crystallographic orientation or domain/grain dimensions in materials with nanoscale order is a critical component of evaluating nanomaterials and their properties. In addition to providing foundations for determining health and safety risks and environmental impact of nanoparticles, these characteristics aid in optimising the properties of emerging nanofabricated materials. For example, phase identification of nanoparticle aerosols and airborne particulates is a key component of evaluating chemical specificity for toxicology/occupational health studies and environmental impact (Friedlander & Pui, 2003). In the nanoelectromechanical systems and nanoelectronics industries, dimensional scaling of materials leads to critical needs for both identification of contaminant particles that can shut down a fabrication line, and characterization of grain structure in ultrathin (<100 nm) films for optimising high-performance, high-reliability devices (International Technology Roadmap for Semiconductors, 2009).

Proven electron diffraction methods such as EBSD in the SEM and convergent-beam electron diffraction (CBED) in the transmission electron microscope (TEM) provide the best chances for generating precise quantitative information about crystallographic orientation, crystal structure or lattice strain from ultrafine domains. However, both techniques face challenges for evaluation of isolated nanoscale volumes such as nanoparticles or single grains in ultrathin films—EBSD lateral spatial resolution in such volumes is typically exceeded at the sub-100 nm scale for isolated particles (Small *et al.*, 2002) and sub-20 nm scale for grains (Maitland & Sitzman, 2007) within ultrathin films due to the backscattered electron interaction volume, especially in directions perpendicular to the tilt axis. Although CBED can provide information from regions of lateral dimensions as small as only a few nanometers, a relatively large specimen thickness is required, in order to cause dynamical contrast within the diffraction disks. This limits the minimum specimen (film or particle) lateral dimension or thickness in a practical sense to several tens of nanometers at best for these techniques, depending on beam energy and atomic number.

Similarly, high-energy transmission Kikuchi diffraction also requires enough specimen thickness [$\sim\frac{1}{2}$ maximum usable

Correspondence to: Robert Keller, NIST Materials Reliability Division, 325 Broadway, Boulder, CO 80305, U.S.A. Tel: +1-303-497-7651; fax: +1-303-497-5030; e-mail: bob.keller@nist.gov

penetration (Edington, 1975)] to cause a sufficient amount of incoherent scattering, in order to generate the new internal sources of diverging electrons that subsequently diffract. From a practical standpoint, this means films or particles must be at least several tens of nanometers thick for 100 keV to 200 keV incident electrons, for low- to mid-range atomic number materials.

Nanobeam spot diffraction in the TEM is capable of producing crystallographic information from regions of lateral diameter of only a few nanometers. For example, long-range order parameters have been measured from nearly equiaxed particles as small as 7 nm by intensity analysis (Sato *et al.*, 2005), and lattice strains have been measured from 3 nm diameter regions of thickness ~250 nm to 300 nm by measuring shifts in spot positions (Vartuli *et al.*, 2007). This method is well suited to analysis of crystallographic characteristics of extremely fine nanoparticles and ultrathin films.

The diffraction patterns presented here very closely resemble EBSD patterns, but are formed in transmission rather than backscattering. Hence, we term the method transmission EBSD, or t-EBSD. To provide context for the new work, we first discuss EBSD in terms of its uses, physics and resolutions (Dingley & Wright, 2009; Humphreys, 2001; Dingley & Randle, 1992). EBSD remains an invaluable tool for characterizing the crystallographic structure of materials in virtually all forms, ranging from structural steel (King *et al.*, 2008) to micro- and nanometer scale particles and films (Small *et al.*, 2002; Geiss *et al.*, 2009). The technique has analytical and spatial resolution limits consistent with electron scattering phenomena in bulk materials.

A conventional EBSD pattern is acquired when the angular intensity variation in electron backscattering from the specimen surface is imaged. The upper specimen surface is tilted towards an angle-sensitive detector, with the specimen normal typically at 70° from the optic axis of the microscope. Kikuchi diffraction takes place, that is, the primary beam scatters incoherently and slightly inelastically within the crystal (Zaefferer, 2007; Winkelmann, 2010), by means of thermal diffuse scattering (TDS), resulting in a new internal divergent electron source that subsequently gives rise to coherently forward scattered electrons that form the diffraction pattern. Intensities in that pattern, which can be calculated by dynamical electron diffraction theory (Reimer *et al.*, 1986; Winkelmann, 2009), are determined by effects of specific atom positions in the unit cell on the probability density for electrons that scatter out of the crystal. For thicker crystals, energy absorption starts to have an effect as well. From a practical standpoint, factors such as degree of local surface roughness or crystal perfection play an important role in determining whether observable Kikuchi bands are detected.

The lateral spatial resolution of EBSD can be viewed as the size of the area of the surface illuminated by the incident beam plus the area out of which electrons are scattered. Factors such as average atomic number and density of the specimen, probe size, and incident electron energy play important roles in determining this resolution. The true physical resolution is typically considered to be of the order of several tens to hundreds of nanometres for bulk materials (Ren *et al.*, 1998; Steinmetz & Zaefferer, 2010; Bhattacharyya & Eades, 2009; Zaefferer, 2007), with the best reported values being in the range of approximately 80 nm to 90 nm perpendicular to the tilt axis and 20 nm to 35 nm parallel to the tilt axis (Zaefferer, 2007; Harland *et al.*, 1981). Depth resolution is thought to depend closely on the nature of the TDS processes taking place during the inelastic event, in terms of both the scattering cross section (Zaefferer, 2007) and location of TDS sources within the sampling volume (Winkelmann, 2010). Depth resolution is highly material-dependent. Measurements of depth resolution in the range of single to a few tens of nanometres have been reported (Zaefferer, 2007; Ren *et al.*, 1998). Dynamical theory suggests that fundamental limits to spatial resolution are approached if sampling volumes dip below 25% of an extinction distance (Deal *et al.*, 2008; Winkelmann, 2010).

Inelastic scattering may also result in detection of electrons that contain no crystallographic information, leading to a background intensity that suppresses both the contrast and sharpness of individual Bragg reflections, especially when scattering arises from depths exceeding the crystallographic information volume (Omoto *et al.*, 2002; Zaefferer, 2007). Such effects impose practical limits on the accuracy of orientation and structure determinations, especially from bulk specimens.

EBSD patterns obtained from thin specimens such as foils or nanoparticles have proven to show higher contrast than those obtained from bulk specimens due to reduction in diffuse scattering from thick mounting substrates. However, acquisition of good quality patterns from extremely fine particles or thin films can be difficult due to the lack of a planar surface, which can cause shadowing effects or direct the beam away from the detector. Further, if specimen dimensions are considerably smaller than the backscattered electron interaction volume for bulk materials, there may be insufficient volume of material available to stimulate a sufficient number of detectable backscattered electrons containing crystallographic information.

Small *et al.* (2002) obtained EBSD patterns of high quality from Al_2O_3 and Fe–Co nanoparticles down to diameters of approximately 120 nm by using a special sample holder that accommodated particles on a TEM specimen grid placed in the common EBSD orientation. Sivel *et al.* (2005) employed a similar approach and demonstrated high quality EBSD patterns from Cu_3Au foils of thickness 100 nm. Such foils were mounted free standing on TEM specimen grids and oriented with foil normal tilted towards the detector. A few observations of transmission electron diffraction from thin specimens have

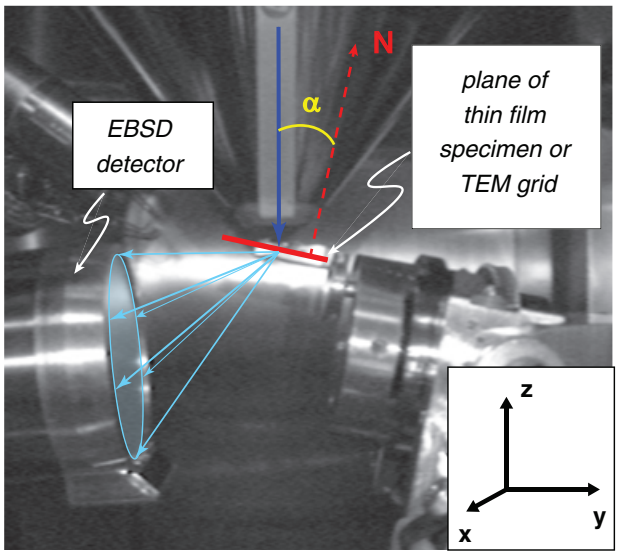

Fig. 1. Infrared image showing relative positions of incident electron beam (dark blue), thin specimen (red), transmitted electrons (light blue) and EBSD camera for collecting t-EBSD patterns in the SEM.

been made in an SEM. An early demonstration of spot pattern formation was provided by Woolf *et al.* (1972), based on the earlier-yet work of Grigson (1961, 1962), using postspecimen scanning coils.

Experimental

The transmission work here is based on the forward-dominance of low energy-loss inelastic scattering (Wells, 1979; Winkelmann, 2010). Conventional EBSD equipment is used to detect and analyse transmitted electrons that have been coherently forward scattered through angles smaller than those associated with conventional EBSD, but larger than those where coherent scattering from the incident beam can dominate.

All t-EBSD data were collected by use of a TSL/EDAX Digiview 1612 high-speed CCD camera with a P-22 high-intensity phosphor, mounted on a LEO 1525 field-emission SEM. Figure 1 shows an infrared image of the specimen-detector geometry used to collect transmission Kikuchi diffraction patterns from a thin film in the SEM; all specimens were mounted on TEM grids. Whereas conventional EBSD requires tilting the specimen surface normal **N** towards the detector, we have tilted our specimen grids in the opposite direction, where **N** moves away from the detector, thereby minimizing backscattering into the detector, and maximizing detection of electrons that have scattered through large angles in transmission. Tilt angles α of approximately 10° to 30° gave rise to a strong signal.

t-EBSD patterns were obtained under a variety of SEM operating conditions, including accelerating voltages in the range 15–30 kV, objective aperture diameter of 60 μm (resulting in a probe current in the range 400–600 pA), and a working distance of 3–12 mm. The EBSD detector was brought to within 30 mm of the specimen/beam intersection. The pattern centre was near the top of the 40 mm diameter phosphor; we found more reliable automated indexing if the pattern centre was located on the phosphor, which required a working distance of 10 mm or more. This configuration resulted in a capture angle of approximately 53° as viewed along the *x*-axis in Figure 1, corresponding to a solid capture angle of 0.66 sr. For this paper, the camera captured 16-bit images at 453 pixels by 453 pixels, typically acquired with an exposure of approximately 1 second. Preliminary studies suggest that shorter exposures typical of those used during automated orientation mapping still result in indexable patterns. Longer exposures and higher pixel-count images resulted in improved signal-to-noise, as expected.

Results

Figure 2(a) shows a secondary electron image of clustered Fe–Co nanoparticles of approximate diameter 10–20 nm. A t-EBSD pattern from particle number 1, with diameter ~10 nm, is shown in Figure 2(b), showing strong contrast and easily indexed reflections. A distinctly different pattern was obtained from particle number 2, and is shown in Figure 2(c). The transmission geometry has resulted in diffraction from Fe–Co particles that are approximately one order of magnitude smaller than those studied by Small *et al.* (2002). Furthermore, the measured particles in Figure 2 are closer together than the spatial resolution typically quoted for EBSD methods.

We note that the contrast of the patterns of Figure 2 is strongly reminiscent of that exhibited by EBSD patterns obtained under typical conditions (bands of bright intensity, band edges of darker intensity, with a somewhat noisy background), and does not show the classic excess-deficit contrast pair observed in TEM-based Kikuchi diffraction. To demonstrate that this is indeed a transmission phenomenon to be distinguished from EBSD, we compare reflection (conventional EBSD) and transmission (t-EBSD) patterns obtained from a nickel film of thickness 40 nm sputter deposited onto a tantalum film of thickness 2.5 nm on an amorphous silicon nitride window of thickness 40 nm; the total specimen thickness was 82.5 nm. Because high angle electron scattering is due primarily to Coulomb interactions with atomic nuclei, with elastic scattering cross section varying with the square of atomic number (Reimer, 1985), we expect that only the nickel contributed significantly to diffraction contrast. The nickel film had a columnar grain structure with mean in-plane grain diameter of 14.5 nm ± 3.6 nm, based on TEM measurements of 195 grains; a bright-field TEM image of this microstructure in plan view is shown in Figure 3(a).

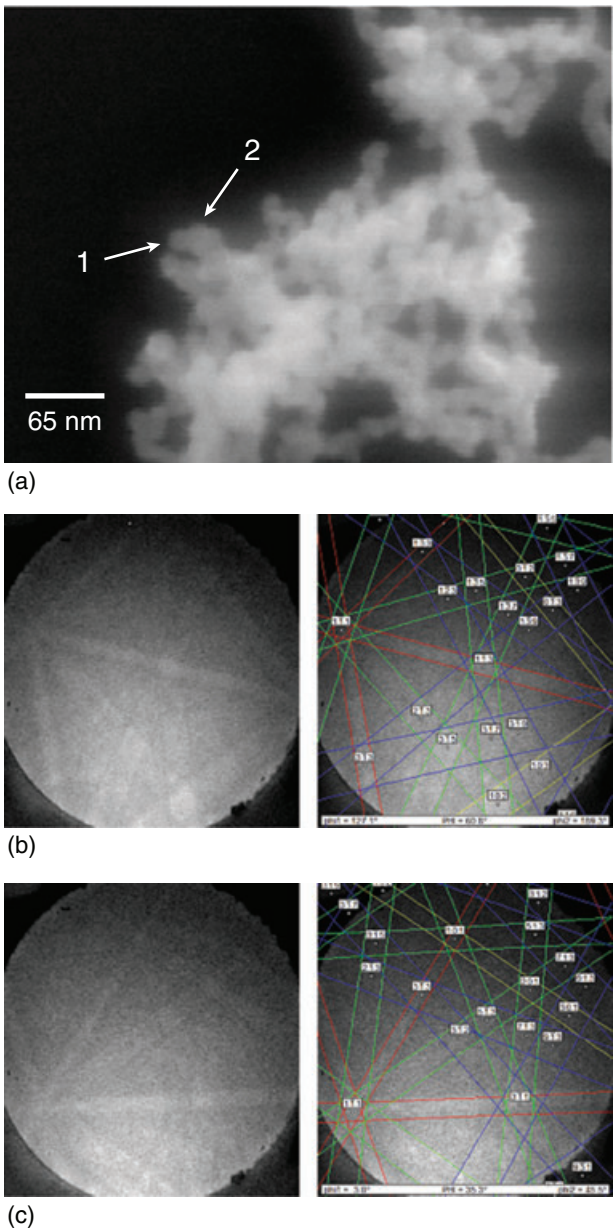

Fig. 2. (a) Secondary electron image of Fe–Co nanoparticles. (b) t-EBSD pattern from particle 1, with indexed pattern on right; particle diameter at this location is approximately 10 nm. (c) t-EBSD pattern from particle 2, with indexed pattern on right; this pattern shows a different orientation from that in Figure 2(b), indicating that particles of diameter 10–20 nm can be distinguished when they are less than 50 nm apart. Beam energy = 20 keV.

Figures 3(b) and (c) show two pairs of images from the EBSD phosphor from this film, each pair taken with the beam positioned 20 nm apart along the specimen surface. The images in Figure 3(b) were obtained using the conventional reflected EBSD configuration; no indexable diffraction patterns were obtained in more than 20 different beam positions. Those in Figure 3(c) were obtained using the transmission

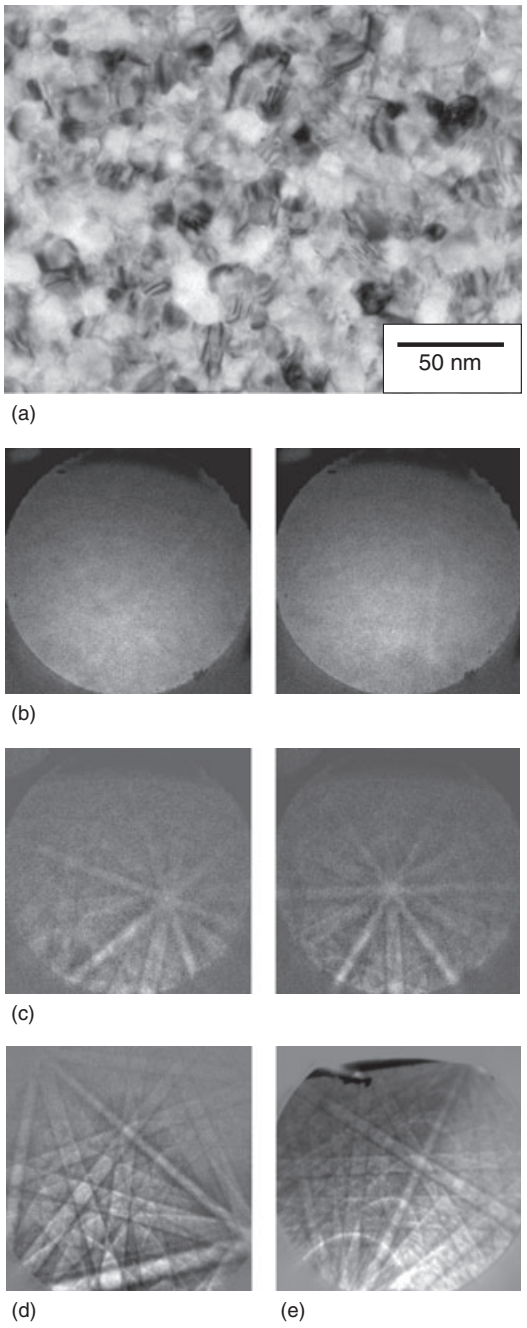

Fig. 3. (a) Bright-field TEM image from ultrathin film specimen of 40 nm nickel/2.5 nm Ta/40 nm amorphous silicon nitride, with mean nickel grain diameter 14.5 nm. (b) Two images of the EBSD phosphor with ultrathin nickel film specimen in conventional EBSD geometry (70° tilt towards detector), with beam positions 20 nm apart. Beam energy = 28 keV. No indexable patterns are visible. (c) Two images of the EBSD phosphor with ultrathin nickel film specimen in transmission EBSD geometry (20° tilt away from detector), with beam positions 20 nm apart; nickel side of specimen downward. Identifiable reflections are observed. (d) Transmission EBSD pattern obtained from ultrathin (50 nm) copper film that was annealed to produce grains larger than those in specimen of Figure 3(a) through Figure 3(c). (e) Transmission EBSD pattern obtained from 50 nm diameter nanowire of GaN.

EBSD configuration, with specimen tilted 20° away from the detector, and the nickel side down. The transmission patterns contain identifiable reflections, with strong contrast, suggesting that the sampling volumes were largely confined to individual grains, even after traversing the amorphous nitride layer. Patterns obtained in that geometry also showed higher average pattern sharpness or 'image quality', a parameter for quantifying the clarity of Kikuchi bands in a pattern. Twenty additional patterns taken in each of the two specimen configurations confirmed that the trend of improved data collection by the transmission method is repeatable over different areas of the film.

Because the patterns of Figure 3(c) appear to be pushing the lateral spatial resolution limits of the t-EBSD method, evidenced by some diffuseness in the reflections, we provide two additional examples of diffraction patterns obtained in transmission to show the quality of reflections that may be obtained in the absence of interference from grain boundaries or multiple crystallites through the specimen thickness. The pattern in Figure 3(d) was obtained from a copper film of thickness 50 nm, which was annealed to provide grains larger than those of the nickel film. The pattern in Figure 3(e) was obtained from a GaN nanowire of approximate diameter 50 nm.

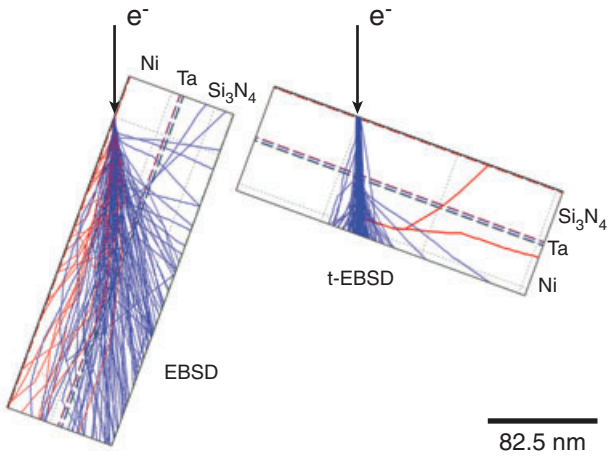

Fig. 4. Monte Carlo simulations (100 000 electrons per simulation) of scattering trajectories for 40 nm nickel/2.5 nm Ta/40 nm amorphous Si_3N_4. Beam energy = 28 keV. Incident beam direction downward in trajectory figures. Trajectories for 100 electrons each in conventional EBSD configuration (left-hand side) and t-EBSD configuration (right-hand side). Red trajectories indicate electrons backscattering out of the incident beam entrance surface. Blue trajectories indicate electrons that have either transmitted through or stopped within the specimen. Note significant difference in interaction volumes.

Discussion

We view t-EBSD as a blend between conventional EBSD and high-energy transmission Kikuchi diffraction, akin to arguments presented by Winkelmann (2010). Emphasis is on scattering within the specimen leading to changes in the propagation direction of electrons, which then coherently forward scatter out of the crystal, through the specimen. Monte Carlo scattering simulations (Drouin *et al.*, 2007) were performed for the polycrystalline nickel specimen to demonstrate the effects of the transmission geometry and specimen tilt away from the detector, focusing on relative differences in signal energy and probe size at the specimen exit surface, as compared to the EBSD configuration. Limitations of this Monte Carlo method focus largely on the neglect of inelastic scattering, resulting in overestimates of energy distributions (Zaefferer, 2007; Winkelmann, 2010).

Figure 4 shows simulated electron trajectories in the EBSD and t-EBSD configurations for an incident beam energy of 28 keV, with a 5 nm diameter incident beam direction downward. The transmission case shows a scattering distribution that exhibits a significantly smaller interaction volume within the specimen than the conventional EBSD case. Rough estimates of the beam diameter at the exit surfaces were made by considering the electron energy losses, as a function of position within the appropriate exit plane of the specimen. Such estimates can be treated as an approximate indication of the extent of beam broadening within the specimen, prior to electron escape, with the assumption that elastic scattering dominates. This assumption may lead to a slight overestimate of the energy distribution (Zaefferer, 2007; Winkelmann, 2010; and perhaps, the extent of broadening), but may still result in reasonable estimates of lateral spatial resolution, especially when comparing in a relative sense.

For the conventional EBSD configuration, we consider as an approximation for lateral spatial resolution the diameter of the area of the top surface out of which backscattered electrons exit, while retaining at least 90% of the primary beam energy. This energy level is consistent with estimates given in references (Ren *et al.*, 1998; Deal *et al.*, 2008), which suggest that such low-loss electrons contribute most strongly to diffraction pattern contrast. The large specimen tilt results in an elongated interaction volume in the direction normal to the tilt axis. We consider the diameter of the escape area in this direction in our resolution estimate. Another consequence of high angles of tilt is the fact that the escape area is displaced somewhat from the precise landing point of the primary beam; from a practical standpoint, this means we must also consider that displacement in estimating spatial resolution. The simulations suggested that low-loss backscattered electrons leave the surface over a range of approximately 80 nm to 150 nm away from the landing position of the primary beam; these electrons emerged from a region of approximate diameter 70 nm, in the direction perpendicular to the specimen tilt axis. However, as indicated above, for practical purposes, the lateral spatial resolution normal to the specimen tilt axis may be considered to include

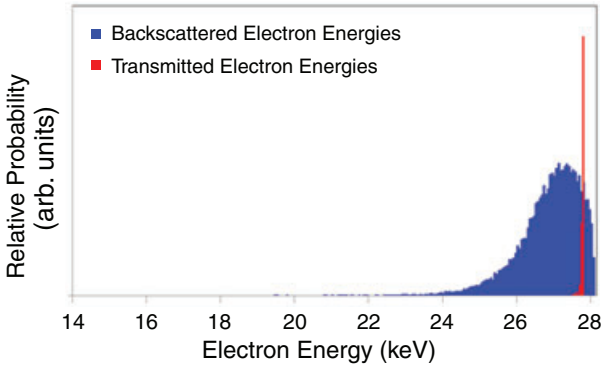

Fig. 5. Scattered-electron energy spectra for backscattered and transmitted electrons, determined by Monte Carlo simulations (100 000 electrons per simulation) for 40 nm nickel/2.5 nm Ta/40 nm Si_3N_4. Beam energy = 28 keV. Note significant differences in mean energies and energy distribution widths.

the region from the primary beam landing position to the furthest extent of escape of low-loss electrons, or 150 nm for this example.

For the transmission configuration, we graphically estimated from scattering trajectories that the full-width half-maximum distribution of the number of electrons exiting the bottom surface of the specimen corresponded to a lateral spacing ranging from about 8 nm to 16 nm for several simulation runs. In the transmission configuration, it may be possible to obtain indexable patterns from particles of diameter even smaller than 10 nm, with a practical lower limit on spatial resolution being approximately one quarter of an extinction distance for the strongest reflections (Deal *et al.*, 2008; Winkelmann, 2010). Figure 5 shows energy spectra for both the backscatter and transmission cases, for incident beam energies of 28 keV. The transmission case notably shows both a higher average energy of ~27.7 keV, compared to ~27.1 keV for the backscatter case, as well as a significantly narrower full-width, half-maximum energy spread of ~0.02 keV, compared to ~1.6 keV for the backscatter case.

Conclusions

A new form of electron backscatter diffraction (EBSD) has been demonstrated in the SEM. Transmission-EBSD presents two primary advantages over conventional EBSD for thin films and nanoparticles: (i) considerably improved lateral spatial resolution, based on electron trajectories at the escape surface, as demonstrated on ~10 nm nanoparticles and grain diameters; this enables analysis of much smaller particles and finer grain size in ultrathin films than that possible by conventional EBSD, (ii) considerably narrowed energy distribution, demonstrated by scattering simulations, potentially enabling analysis of finer structure within the diffraction pattern for more sophisticated structure determination than that currently possible with conventional EBSD patterns. Higher average energy and significantly narrower energy spread suggest there is considerably less multiple scattering in the transmission case, leading to less pattern blurring from small sampling volumes, consistent with recent findings showing the use of energy filtering to improve EBSD spatial resolution (Bhattacharyya & Eades, 2009). Other applications of the t-EBSD method, including orientation mapping of films prepared by focused ion beam milling, will be compared to conventional EBSD maps and addressed in forthcoming work. We anticipate trade-offs between superior spatial resolution in transmission and larger sampling areas in reflection, due to limitations associated with thin specimen preparation. This new technique adds a diffraction capability to an emerging arena of high spatial resolution transmission imaging and analysis within energy regimes dominated by the SEM (Day, 2009; Joy, 2009; Zhu *et al.*, 2009).

Acknowledgements

We thank the NIST Office of Microelectronics Programs for support, and Justin Shaw, NIST Electromagnetics Division, for fabricating silicon nitride membranes. Commercial equipment, instruments or materials are identified in order to adequately specify certain procedures. In no case does such identification imply recommendation or endorsement by the National Institute of Standards and Technology, nor does it imply that the products identified are necessarily the best available for the purpose.

References

International Technology Roadmap for Semiconductors (2009) Edition. (ed. SEMATECH) (http://www.itrs.net).

Bhattacharyya, A. & Eades, J.A. (2009) Use of an energy filter to improve the spatial resolution of electron backscatter diffraction. *Scanning* **31**, 114–121.

Day, A.P. (2009) Spherical Kikuchi maps and other rarities. *Electron Backscatter Diffraction in Materials Science* (ed. by A. Schwartz, M. Kumar, B. Adams & D.P. Field), pp. 65–80. Springer Science + Business Media, New York.

Deal, A., Hooghan, T. & Eades, A. (2008) Energy-filtered electron backscatter diffraction. *Ultramicroscopy*. **108**, 116–125.

Dingley, D.J. & Randle, V. (1992) Microtexture determination by electron back-scatter diffraction. *J. Mater. Sci.* **27**, 4545–4566.

Dingley, D.J. & Wright, S.I. (2009) Determination of crystal phase from an electron backscatter diffraction pattern. *J. Appl. Crystallogr.* **42**, 234–241.

Drouin, D., Couture, A.R., Joly, D., Tastet, X., Aimez, V. & Gauvin, R. (2007) CASINO V2.42 – A fast and easy-to-use modeling tool for scanning electron microscopy and microanalysis users. *Scanning* **29**, 92–101.

Edington, J.W. (1975) Electron diffraction in the electron microscope. *Practical Electron Microscopy in Materials Science*, p. 11. Philips, Eindhoven.

Friedlander, S.K. & Pui, D.Y.H. (2003) NSF Workshop Report on Emerging Issues in Nanoparticle Aerosol Science and Technology (NAST). UCLA, Los Angeles.

Geiss, R.H., Read, D.T., Alers, G.B. & Graham, R.L. (2009) EBSD analysis of narrow damascene copper lines. *Frontiers of Characterization and Metrology for Nanoelectronics: 2009* (eds. D.G. Seiler, A.C. Diebold, R. McDonald, C.M. Garner, D. Herr, R.P. Khosla & E.M. Secula), pp. 154–158. Amer Inst Physics, Melville.

Grigson, C. W.B. (1961) High-speed direct-recording system for electron diffraction. *Nature* **192**, 647–648.

Grigson, C. W.B. (1962) On scanning electron diffraction. *J. Electron. Control* **12**, 209–232.

Harland, C.J., Akhter, P. & Venables, J.A. (1981) Accurate microcrystallography at high spatial resolution using electron back-scattering patterns in a field emission gun scanning electron microscope. *J. Phys. E: Sci. Instrum.* **14**, 175–182.

Humphreys, F.J. (2001) Grain and subgrain characterisation by electron backscatter diffraction. *J. Mater. Sci.* **36**, 3833–3854.

Joy, D.C. (2009) Scanning electron microscopy – second best no more. *Nat. Mater.* **8**, 776–777.

King, A., Johnson, G., Engelberg, D., Ludwig, W. & Marrow, J. (2008) Observations of intergranular stress corrosion cracking in a grain-mapped polycrystal. *Science* **321**, 382–385.

Maitland, T. & Sitzman, S. (2007) Electron backscatter diffraction (EBSD) technique and materials characterization examples. *Scanning Microscopy for Nanotechnology Techniques and Applications* (eds. by W. Zhou & Z. L. Wang), pp. 41–75. Springer, New York.

Omoto, K., Tsuda, K. & Tanaka, M. (2002) Simulations of Kikuchi patterns due to thermal diffuse scattering on MgO crystals. *J. Electron Microsc.* **51**, 67–78.

Reimer, L. (1985) *Scanning Electron Microscopy, Physics of Image Formation and Microanalysis*. 1st edn, pp. 57–73. Springer-Verlag, New York.

Reimer, L., Heilers, U. & Saliger, G. (1986) Kikuchi band contrast in diffraction patterns recorded by transmitted and backscattered electrons. *Scanning* **8**, 101–118.

Ren, S.X., Kenik, E.A., Alexander, K.B. & Goyal, A. (1998) Exploring spatial resolution in electron back-scattered diffraction experiments via Monte Carlo simulation. *Microsc. Microanal.* **4**, 15–22.

Sato, K., Hirotsu, Y., Mori, H., Wang, Z. & Hirayama, T. (2005) Long-range order parameter of single L1o-FePd nanoparticle determined by nanobeam electron diffraction: particle size dependence of the order parameter. *J. Appl. Phys.* **98**, 024308-1–024308-8.

Sivel, V.G.M., Tichelaar, F.D., Mohdadi, H., Alkemade, P.F.A. & Zandbergen, H.W. (2005) Crystallographic analysis of thin specimens. *J. Microsc.* **218**, 115–124.

Small, J.A., Michael, J.R. & Bright, D.S. (2002) Improving the quality of electron backscatter diffraction (EBSD) patterns from nanoparticles. *J. Microsc.* **206**, 170–178.

Steinmetz, D.R. & Zaefferer, S. (2010) Towards ultrahigh resolution EBSD by low accelerating voltage. *Mater. Sci. Technol.* **26**, 640–645.

Vartuli, C.B., Jarausch, K., Inada, H., Tsuneta, R., Dingley, D.J. & Marley, E.A. (2007) Strain measurements using nano-beam diffraction on a FE-STEM. *Microsc. Microanal.* **13**, 836–837.

Wells, O.C. (1979) Effects of collector take-off angle and energy filtering on the BSE image in the SEM. *Scanning* **2**, 199–216.

Winkelmann, A. (2009) Dynamical simulation of electron backscatter diffraction patterns. In: *Electron Backscatter Diffraction in Materials Science* (eds. by A. Schwartz, M. Kumar, B. Adams & D. Field), pp. 21–33. Springer Science+Business Media, New York.

Winkelmann, A. (2010) Principles of depth-resolved Kikuchi pattern simulation for electron backscatter diffraction. *J. Microsc.* **239**, 32–45.

Woolf, R.J., Joy, D.C. & Tansley, D.W. (1972) A transmission stage for the scanning electron microscope. *J. Phys. E: Sci. Instrum.* **5**, 230–233.

Zaefferer, S. (2007) On the formation mechanisms, spatial resolution and intensity of backscatter Kikuchi patterns. *Ultramicroscopy* **107**, 254–266.

Zhu, Y., Inada, H., Nakamura, K. & Wall, J. (2009) Imaging single atoms using secondary electrons with an aberration-corrected electron microscope. *Nat. Mater.* **8**, 808–812.

